Behavioural and functional characterization of Kv10.1 (Eag1) knockout mice

Roser Ufartes[1],*,[†], Tomasz Schneider[4],[†], Lena Sünke Mortensen[2], Camino de Juan Romero[5], Klaus Hentrich[6], Hendrik Knoetgen[7], Vadim Beilinson[8], Wiebke Moebius[3], Victor Tarabykin[9], Frauke Alves[1],[10], Luis A. Pardo[1], J. Nicholas P. Rawlins[4] and Walter Stuehmer[1]

[1]Department of Molecular Biology of Neuronal Signals, [2]Department of Molecular Neurobiology, [3]Department of Neurogenetics, Max-Planck-Institute of Experimental Medicine, Göttingen 37075, Germany, [4]Experimental Psychology, University of Oxford, South Parks Road, Oxford OX1 3UD, UK, [5]Instituto de Neurociencias, CSIC & Universidad Miguel Hernández, Sant Joan d'Alacant 03550, Spain, [6]The Maynard Centre, GE Healthcare Life Sciences, Cardiff CF14 7YT, UK, [7]Pharma Research and Early Development, Roche Diagnostics GmbH, Penzberg 82377, Germany, [8]Bayer CropScience, 3500 Paramount Parkway, Morrisville, NC 27560, USA, [9]Institute of Cell Biology and Neurobiology, Neurocure Cluster of Excellence, Charité–Universitätsmedizin Berlin, Campus Mitte, Berlin 10117, Germany and [10]Department of Hematology and Oncology, University Medical Center Göttingen, Göttingen 37075, Germany

Kv10.1 (Eag1), member of the Kv10 family of voltage-gated potassium channels, is preferentially expressed in adult brain. The aim of the present study was to unravel the functional role of Kv10.1 in the brain by generating knockout mice, where the voltage sensor and pore region of Kv10.1 were removed to render non-functional proteins through deletion of exon 7 of the KCNH1 gene using the '3 Lox P strategy'. Kv10.1-deficient mice show no obvious alterations during embryogenesis and develop normally to adulthood; cortex, hippocampus and cerebellum appear anatomically normal. Other tests, including general health screen, sensorimotor functioning and gating, anxiety, social behaviour, learning and memory did not show any functional aberrations in Kv10.1 null mice. Kv10.1 null mice display mild hyperactivity and longer-lasting haloperidol-induced catalepsy, but there was no difference between genotypes in amphetamine sensitization and withdrawal, reactivity to apomorphine and haloperidol in the prepulse inhibition tests or to antidepressants in the haloperidol-induced catalepsy. Furthermore, electrical properties of Kv10.1 in cerebellar Purkinje cells did not show any difference between genotypes. Bearing in mind that Kv10.1 is overexpressed in over 70% of all human tumours and that its inhibition leads to a reduced tumour cell proliferation, the fact that deletion of Kv10.1 does not show a marked phenotype is a prerequisite for utilizing Kv10.1 blocking and/or reduction techniques, such as siRNA, to treat cancer.

INTRODUCTION

The *Drosophila ether-à-go-go* (*eag*) gene is the founding member of an evolutionarily conserved superfamily of voltage-gated potassium channels with homology to cyclic nucleotide-gated channels (1–3). Mutations in *eag* in adult flies cause ether-induced shaking (4,5) and memory formation defects (6). The effects of *eag* mutations in *Drosophila* appear not entirely dependent on ion permeation, but rather on interaction with MAPK (7). One of the hallmark features of hKv10.1 channels is their sensitivity to intracellular Ca^{2+} mediated by calmodulin (CaM) (8), through the Ca^{2+}/CaM binding domain (9–11). Mutation in this domain reduced inhibition of the functional channel by Ca^{2+}/CaM (10,11).

*To whom correspondence should be addressed at: Department of Molecular Biology of Neuronal Signals, Max-Planck-Institute for Experimental Medicine, Hermann-Rein-Str. 3, Göttingen 37077, Germany. Tel: +49 05513899272; Fax: +49 05513899644; Email: rufarte@gwdg.de
[†]The authors wish it to be known that, in their opinion, the first two authors should be regarded as joint First Authors.

Mammalian genomes contain at least seven orthologs of the *eag* subfamily. Two members, $K_v10.1$ (Eag1) (12,13) and $K_v10.2$ (Eag2) (8,14), share about 70% identity in amino acid sequence (8). In adult mammals, the expression of $hK_v10.1$ channels is restricted to the nervous system (13); however, $hK_v10.1$ is found in over 70% of all human tumour tissues (15–23) making $K_v10.1$ an attractive target for the development of diagnostic and therapeutic tools in oncology (24). Their function in brain and during tumour development and progression still needs to be elucidated.

In brains of adult rats, $K_v10.1$ shows the highest mRNA expression in olfactory bulb, cerebral cortex, hippocampus and cerebellum (8,25); mRNA expression is highly correlated with detection of $K_v10.1$ protein (26). Given that $K_v10.1$ appears largely neuron specific and localized at synapses (27), $K_v10.1$ signalling may regulate activity-dependent changes in neuronal function such as the excitability and firing dynamics of Purkinje cells (PCs) that expressed $K_v10.1$, but not its paralogue $K_v10.2$ (8,25,28).

Although a correlation of $K_v10.1$ to neurological disorder has not been described yet, an evidence for a schizophrenia-susceptibility locus in $K_v10.1$ region was found in a genome-wide genetic linkage analysis (29). These results are consistent with first immunohistochemical analysis of human brain sections that showed lower protein expression of $K_v10.1$ in the frontal cortex and hippocampus of patients suffering from schizophrenia in comparison to non-schizophrenic subjects (S. Martin, personal communication).

Potassium channels, including $K_v10.1$, have also been implicated in antidepressant action (30–32). Imipramine blocks $K_v10.1$ channels by occluding the permeation pathway and possibly affects the cell cycle (32); this offers a potential mechanism by which imipramine causes a significant reduction in melanoma cells proliferation (33).

Therefore, the aim of this study was to investigate the functional role of $K_v10.1$ in brain *in vivo* using behavioural, morphological and electrophysiological characterization of $K_v10.1$-deficient mice generated by the '3 Lox P strategy'. In these mice the voltage sensor and pore region of Kv10.1 were removed to render non-funtional proteins. To this aim, general health screening and behaviour studies were performed, including sensorimotor functioning and gating, anxiety, social behaviour, learning and memory, AMPH sensitization, haloperidol-induced catalepsy and its modification by antidepressants as well as disruption of prepulse inhibition by apomorphine and its reversal by haloperidol. We report that $K_v10.1$-deficient mice display mild hyperactivity and longer lasting haloperidol-induced catalepsy in comparison to controls, but otherwise normal behaviour, and no obvious histological changes or differences in electrophysiological responses in the cerebellum.

RESULTS

Generation and characterization of $K_v10.1$-deficient mice

To determine the physiological role of $K_v10.1$ *in vivo*, we generated $K_v10.1$-deficient mice by homologous recombination in embryonic stem (ES) cells to disrupt part of the $K_v10.1$ gene (Fig. 1A). To avoid the possibility of early lethality of total

$K_v10.1$-deficient mice, the '3 Lox P strategy' was used to generate total and conditional knockout mice. We screened a mouse genomic library in lambda phages (Stratagene) to isolate a fragment of mouse genomic DNA encompassing the entire Exon 7, which encodes amino acid residues 344–388 of the $K_v10.1$ peptide, that was chosen as the targeting region to produce non-functional $K_v10.1$ proteins. Exon 7 encodes the voltage sensor and pore-lining regions of $K_v10.1$; with this deletion, even in the case of unknown alternative splicing or transcription start sites, the resulting protein would lack voltage dependence and ion permeability. A replacement vector was designed to introduce three tandem repeats of Lox P sites flanking both ends of Exon 7 and a neomycin resistance (Neo) selection cassette. ES cells were transfected and selected for homologous recombination through positive (Neo) and negative (HSV-tk) double selection (Fig. 1A). Recombinant ES clones were selected by Southern Blot analysis (Fig. 1B), injected into blastocysts and transferred into a pseudo-pregnant foster mother. Mice heterozygous for the lox P-flanked $K_v10.1$ locus and for the Neo cassette $K_v10.1^{NeoLoxP}$ were obtained after breeding the resulting male chimeras with C57BL6/N females. To get *in vivo* partial (floxed allele) and/or total excision (null allele) of Lox P-flanked sequence in the targeted loci, heterozygous mice were crossed with *Ella*Cre transgenic mice that provide an early expression of Cre recombinase during embryogenesis. The absence of both $K_v10.1$ mRNA and $K_v10.1$ protein in the knockout mice was confirmed by real time RT-PCR and western blot analyses [previously described (26)]. As shown in Figure 1C, no $K_v10.1$ product was amplified from $K_v10.1^{-/-}$ brain, whereas $K_v10.1^{+/-}$ mice expressed approximately half of the amount of $K_v10.1$ message found in the brain of $K_v10.1^{+/+}$ mice. Western blot analysis using proteins isolated from total brain of $K_v10.1^{+/+}$ and of $K_v10.1^{-/-}$ mice did not detect $K_v10.1$ in $K_v10.1^{-/-}$ mice (Fig. 1D). Importantly, we did not detect an increase in the expression of the closely related potassium channel $K_v10.2$ at the RNA level by real time RT-PCR in response to the absence of $K_v10.1$ expression (Fig. 1E). Possible genetic compensation was assessed by microarray analysis on hippocampal cDNA of $K_v10.1^{+/+}$ and $K_v10.1^{-/-}$ (Supplementary Material, Table S1); except for the targeted gene itself, no significant differences were observed between the samples.

$K_v10.1^{-/-}$ mice are viable and fertile and display a morphologically normal brain

Genotyping of litters from intercrosses of F1 $K_v10.1^{+/-}$ revealed that $K_v10.1^{-/-}$ mice appeared in Mendelian ratios. From 200 mice, 25% were $K_v10.1^{+/+}$, 49% were $K_v10.1^{+/-}$ and 26% were $K_v10.1^{-/-}$, indicating no embryonic lethality of $K_v10.1^{-/-}$. Breeding studies also indicate that $K_v10.1^{-/-}$ mice could interbreed, proving that they are fertile (Data not shown).

Detailed histological analysis of Nissl-stained brain sections and immunohistochemical analysis of adjacent sections with antibodies directed against neuronal markers, including the calcium-binding proteins calbindin and calretinin and neuronal nuclei (NeuN), did not reveal any significant differences of morphology between $K_v10.1^{+/+}$ and $K_v10.1^{-/-}$. The structure
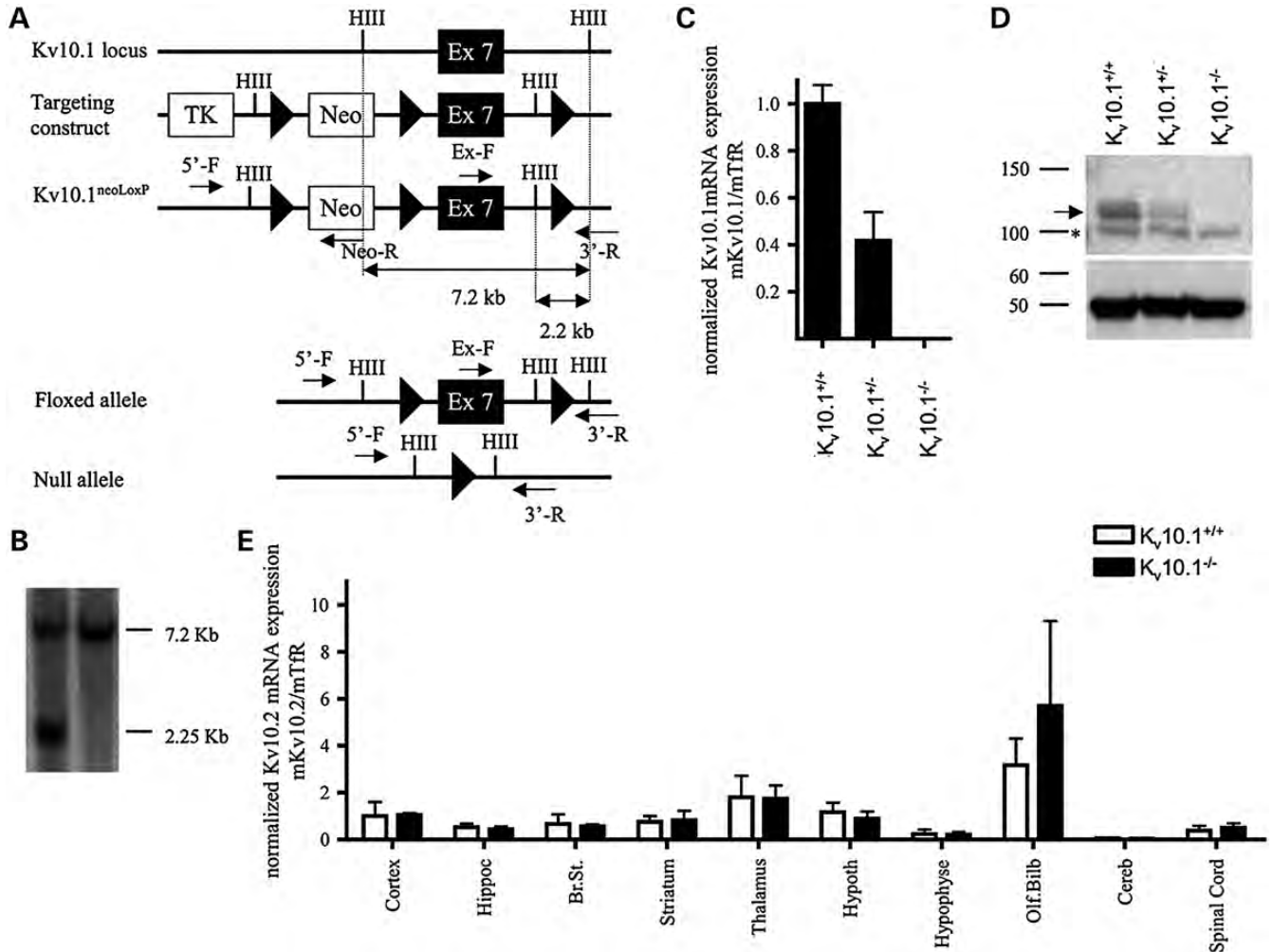
Figure 1. Generation and expression analysis of $K_v10.1$-deficient mice. (**A**) Schematic representation of the $K_v10.1^{+/+}$ locus, the targeting construct and the mutated alleles. $K_v10.1^{neoLoxP}$ were bred with *Ella*Cre transgenic mice to produce *in vivo* floxed allele and/or null allele due to an early expression of Cre re-combinase during mouse embryo development. The probe for Southern blot analysis and primers for genotyping are indicated. (**B**) Southern blot analysis of $K_v10.1$-ES cells (*Hin*dIII digested) is shown. Bands corresponding to the different alleles are indicated (wild-type allele: 7.2 Kb $K_v10.1$; recombinant allele: 2.25 Kb $K_v10.1$). (**C**) Real time RT–PCR on cDNA was obtained from total brain RNA in $K_v10.1^{+/+}$, $K_v10.1^{+/-}$ and $K_v10.1^{-/-}$ mouse. The results indicate a compete deletion of $K_v10.1$ on $K_v10.1^{-/-}$ animals. (**D**) Western blot using a polyclonal anti-$K_v10.1$ antibody did not detect specific signals in brain $K_v10.1^{-/-}$ mice. The filled arrowhead marks the expected position for $K_v10.1$; non-specific bands are marked by an asterisk. Open arrowhead shows α-tubulin used as a control. (**E**) Real time RT–PCR on cDNA obtain from cortex, hippocampus, brain stem, striatum, thalamus, hypothalamus, hypophysis, olfactory bulb, cerebel-lum and spinal cord from $K_v10.1^{+/+}$ and $K_v10.1^{-/-}$ mice. Kv10.2 expression is not regulated due to the absence of $K_v10.1$ in $K_v10.1^{-/-}$ mice.

and layering of the cortex shown by Nissl and NeuN staining were indistinguishable for both genotypes (Fig. 2A–D), and no evident difference could be detected in the organization of the hippocampus (Fig. 2E and F). Nissl, calbindin and cal-retinin staining indicate that PCs, molecular layer dendrites and axonal fibres in the cerebellum appeared unchanged in both genotypes (Fig. 2G–L). Electron microscopy analysis of the parallel fibre to PC dendrite synapses in the molecular layer also revealed no obvious differences (Fig. 2M and N).

Electrical properties of $K_v10.1$ in cerebellar PCs

Voltage-gated potassium channels play various important roles in the central nervous system such as modulation of the resting potential, control of excitability and repolarization of the membrane after an action potential (34). $K_v10.1$

activates close to the resting potential (12). Therefore, we decided to investigate its implication in determining the resting potential and excitability of cerebellar PCs that express $K_v10.1$ (26). PCs under whole-cell patch clamp in current clamp mode were held close to -60 mV by current in-jection. On further injection of a depolarizing current, cells from both genotypes showed tonic firing of action potentials. Figure 3A shows a typical recording from a $K_v10.1^{+/+}$ (top) and $K_v10.1^{-/-}$ (middle) cell and a representative action po-tential recorded in a $K_v10.1^{+/+}$ (bottom left) and $K_v10.1^{-/-}$ (bottom right) cell. Without current injection, V_{mem} was -63.90 ± 3.33 mV ($n = 8$) in $K_v10.1^{+/+}$ cells versus -54.78 ± 2.31 mV ($n = 8$) in $K_v10.1$-deficient cells. However, because the potential measured by whole-cell patch clamp is influenced by the quality of the preparation and the damage to the cell caused by the patch pipette, these
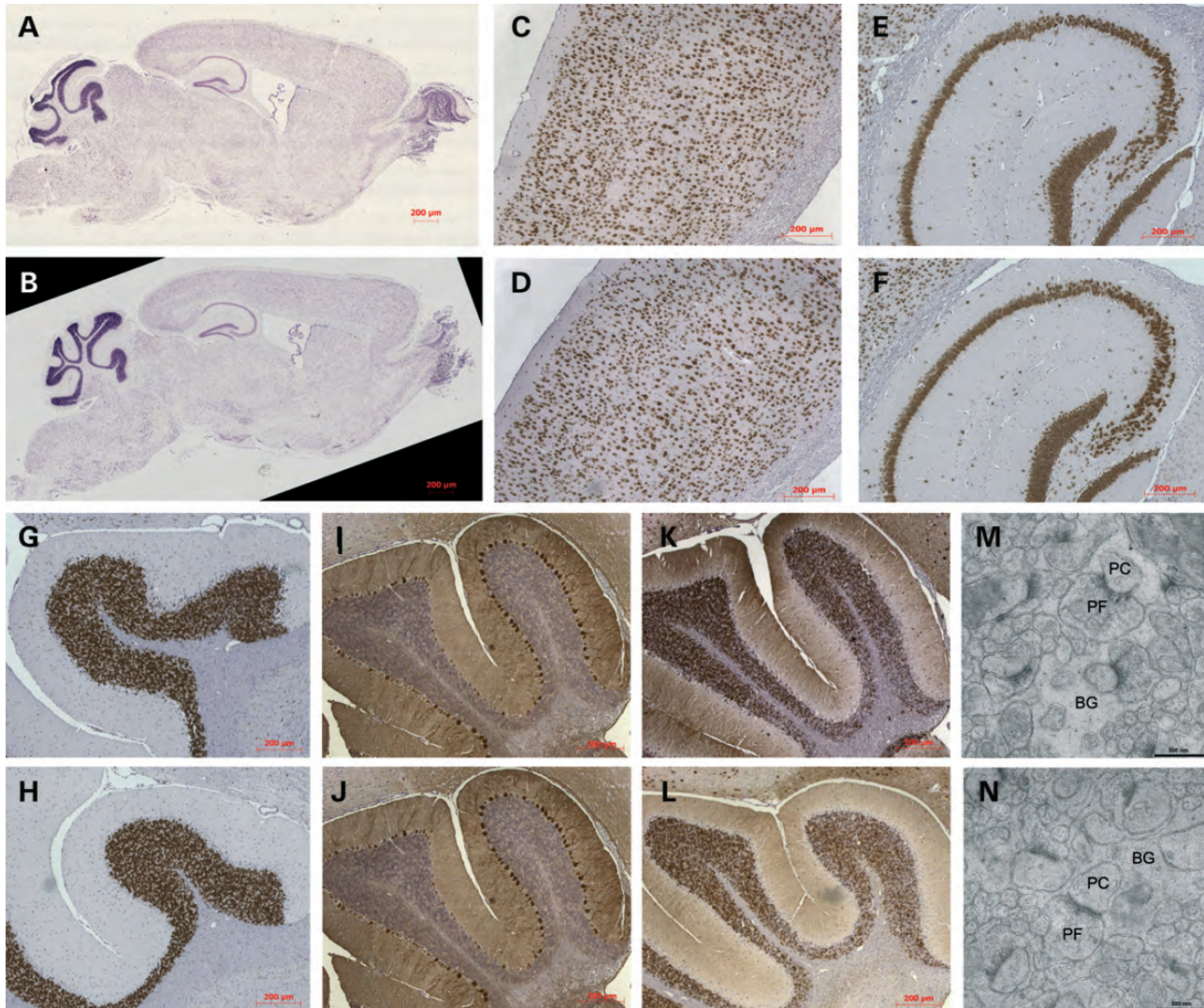
Figure 2. Normal morphology of the brain of $K_v10.1^{-/-}$ mice. Nissl staining of comparable sagittal brain sections from $K_v10.1^{+/+}$ (**A**) and $K_v10.1^{-/-}$ (**B**) (5 μm, paraffin). Representative images of sagital brain sections at $10\times$ magnification stain with NeuN of the neocortex and hippocampus ($K_v10.1^{+/+}$: **C** and **E**; $K_v10.1^{-/-}$: **D** and **F**). Representative images of cerebellum stained with NeuN ($K_v10.1^{+/+}$: **G**; $K_v10.1^{-/-}$: **H**), calbindin ($K_v10.1^{+/+}$: **I**; $K_v10.1^{-/-}$: **J**) and calretinin ($K_v10.1^{+/+}$: **K**; $K_v10.1^{-/-}$: **L**). *Scale bar* 200 μm. Morphology of the parallel fibre to PC dendrite synapses in the molecular layer appears normal in $K_v10.1^{+/+}$ (**M**) and $K_v10.1^{-/-}$ (**N**) using electron microscopy. BG, Bergmann glia. *Scale bar*, 500 nm.

results need to be interpreted carefully. To calculate the input resistance, we injected square current pulses (-100 to $+100$ pA in steps of 20 pA) into the soma and recorded the resulting changes in membrane voltage. The obtained current−voltage (I−V) relationship for hyperpolarizing current injection is close to linear with the slope representing the membrane resistance (35). Neither the obtained values for V_{mem} nor the slope of the fit were significantly different between $K_v10.1^{+/+}$ (solid circles) and $K_v10.1^{-/-}$ cells (open circles) (Fig. 3B).

Next, we examined whether injection of depolarizing voltage pulses leads to changes in the firing frequencies of PCs. Cells were held close to -60 mV in current clamp mode, and square current pulses ranging from -100 to $+100$ pA in steps of 10 pA and from $+100$ to $+1000$ pA in steps of 50 pA were injected. The minimal current injection

to elicit an action potential was not significantly different in $K_v10.1^{+/+}$ and $K_v10.1^{-/-}$ cells (104.0 ± 38.68pA, $n = 5$ and 61.67 ± 21.51, $n = 6$). Spikes were detected as a local maximum, and the resulting spike frequencies were plotted against the injected current (Fig. 3C). $K_v10.1^{-/-}$ neurons showed slightly, but not significantly, increased evoked firing frequencies in comparison to $K_v10.1^{+/+}$ cells on injection of currents < 100 pA. To evaluate whether $K_v10.1$ is involved in shaping the action potential, the first 10 action potentials occurring after breaking the membrane were averaged and analysed for each cell (Fig. 3D). The comparison of the after hyperpolarization (i), full width at half maximum (ii), overshoot (iii) and threshold (iv) of the action potential revealed no significant differences between $K_v10.1^{-/-}$ neurons and $K_v10.1^{+/+}$ cells. Equivalent results were obtained when comparing the electrophysiological
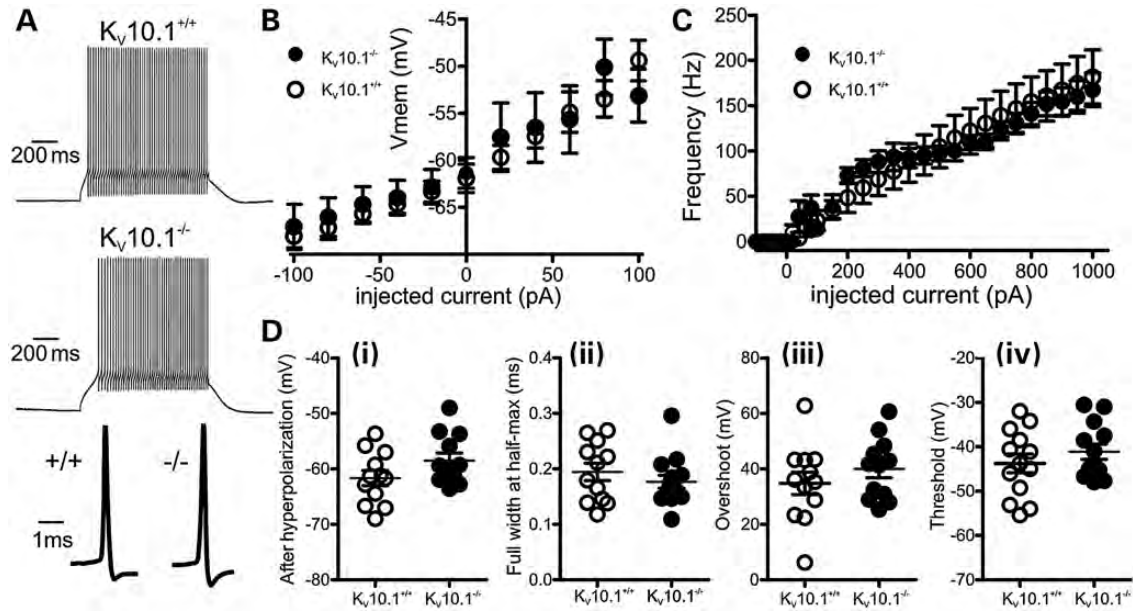
Figure 3. Electrophysiological properties of cerebellar PCs of $K_v10.1^{+/+}$ and $K_v10.1^{-/-}$ mice. (**A**) *top*, representative recordings of a spike train in response to a superthreshold current injection in a PC from a $K_v10.1^{+/+}$ mouse. *Centre*, same from a $K_v10.1^{-/-}$ mouse. *Bottom*, representative action potentials recorded in $K_v10.1^{+/+}$ (*left*) and $K_v10.1^{-/-}$ (*right*) cells. (**B**) Membrane voltage in response to current injections ranging from -100 to $+100$ pA in steps of 20 pA as measured in the cell bodies of $K_v10.1^{+/+}$ (*solid circles*) and $K_v10.1^{-/-}$ (*open circles*) PCs. (**C**) Firing frequencies of $K_v10.1^{+/+}$ (*solid circles*) and $K_v10.1^{-/-}$ (*open circles*) PCs in response to somatic current injection ranging from -100 to $+100$ pA in 10 pA steps and from $+100$ to $+1000$ pA in 50 pA increments. (**D**) Action potential properties of $K_v10.1^{+/+}$ (*solid circles*) and $K_v10.1^{-/-}$ (*open circles*) PCs. The first 10 spontaneously occurring action potentials were averaged in a given cell and after hyperpolarization (i), full width at half maximum (ii), overshoot (iii) and threshold (iv) were compared.

properties of hippocampal granule cells from Kv10.1$^{-/-}$ ($n = 8$) and Kv10.1$^{+/+}$ ($n = 4$) mice (Data not shown).

Behavioural tests

Mild hyperactivity in $K_v10.1$-deficient mice

To document general health, we determined 16 parameters, including, e.g. body weight, coat condition, motoric abilities, reflexes, reactivity to handling, spontaneous behaviours and olfaction (for the full list of tests and results, see Table 1); we found no differences between genotypes in any of these parameters.

There was a non-significant tendency towards a main effect of genotype on spontaneous locomotor activity during a 60 min test session [$F(1,29) = 3.51$, $P < 0.07$] and a significant genotype × within session period interaction [$F(11,23) = 2.33$, $P < 0.01$]. $K_v10.1^{-/-}$ mice were more active during all 5 min periods except for the first 15 min (*post hoc* tests, minimum $P < 0.03$). This difference tended to increase as testing continued (Fig. 4A). There was no difference between genotypes in coordination and motor learning in the rotarod test [Fig. 4B; $F(1,29) = 0.005$, n.s.]. Both genotypes improved their performance on consecutive tests [$F(2,29) = 22.51$, $P < 0.0001$].

Short-term effects of amphetamine (AMPH) withdrawal in $K_v10.1^{-/-}$ mice

Amphetamine (AMPH) withdrawal had no impact on anxiety (Table 2, light-dark box) or social behaviour (Table 3), but

Table 1. General health screening

	$K_v10.1^{+/+}$	$K_v10.1^{-/-}$
General health		
Body weight (g)	21.71 ± 0.27	22.34 ± 0.34
Poor coat condition (%)	0	0
Bald patches (%)	0	0
Missing whiskers (%)	0	0
Piloerection (%)	0	0
Physical abnormalities (%)	0	0
Motoric abilities		
Trunk curl (%)	69	73
Forepaw reaching (%)	100	100
Inverted screen (s)	60	60
Reflexes (% of mice normal)		
Ear twitch (%)	100	100
Whisker twitch (%)	100	100
Reactivity		
To handling (three-point scale)	0.94	1
Empty cage behaviour (3 min test)		
Freezing (%)	0	0
Wild running (%)	0	0
Grooming (s)	6.04 ± 0.73	8.92 ± 1.66
Grooming (events)	3.06 ± 0.49	3.6 ± 0.65
Olfaction (3 min test; diluted oil drop on the wall)		
Sniffing time (s)	6.72 ± 0.74	5.1 ± 0.94
Number of sniffs	5.63 ± 0.69	4.8 ± 0.49
Latency to first sniff (s)	38.74 ± 7.84	31.53 ± 7.48

There were no significant between genotype differences in tests measuring animals' general health and sensorimotor abilities (for details, see Materials and Methods). Data are shown as mean $\pm$ SEM; $n = 15-16$ per group. There was no between groups difference in any of the above parameters.
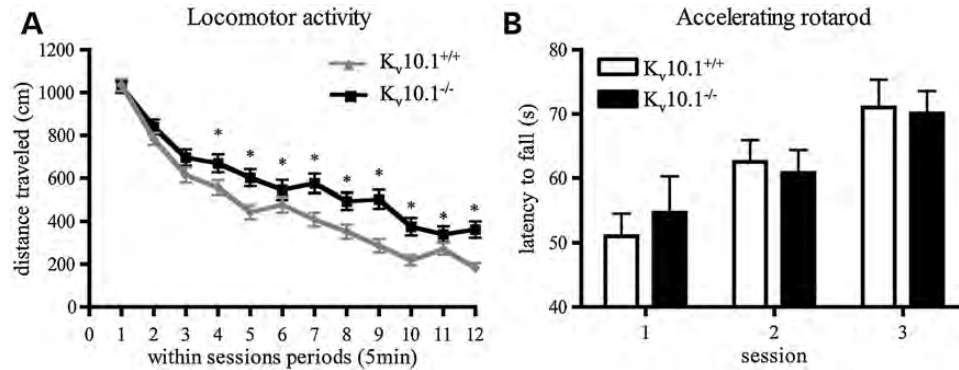
Figure 4. Increased spontaneous activity (**A**) and normal motor coordination and motor learning in the rotarod test (**B**) in $K_v10.1^{-/-}$ mice (for details, see Materials and Methods). Data are shown as mean + SEM; $n = 15–16$ per group. * $P < 0.05$ versus $K_v10.1^{+/+}$.

Table 2. Anxiety

Test/parameter	$K_v10.1^{+/+}$	$K_v10.1^{-/-}$	$K_v10.1^{+/+}$AMPH	$K_v10.1^{-/-}$ AMPH
Light/dark box		Within 6 days after AMPH withdrawal		
Transitions	18 ± 2.36	25 ± 1.58	18.88 ± 1.23	19.14 ± 1.37
Latency to enter the dark side (s)	8.33 ± 2.09	9.71 ± 2.53	17.07 ± 5.70	12.87 ± 3.59
Distance travelled (cm)	931.35 ± 105.52	1012.06 ± 83.69	1035.11 ± 100.36	1000.43 ± 118.09
Time in dark zone (s)	434.18 ± 18.78	396.08 ± 23.99	416.09 ± 27.38	448.86 ± 11.80
Elevated plus maze		3 weeks after AMPH withdrawal		
Open arms entries (%)	24.89 ± 3.58	24.66 ± 4.24	20.33 ± 3.12	21.13 ± 3.39
Time in open arms (%)	5.44 ± 1.10	7.03 ± 1.68	7.31 ± 2.26	4.63 ± 1.56
Closed arms entries	11.50 ± 2.01	12 ± 2.17	11.50 ± 1.52	7.71 ± 1.44
Hyponeophagia		3 weeks after AMPH withdrawal		
Latency to eat (s)	202.13 ± 47.52	288.88 ± 45.12	211.25 ± 49.93	253.86 ± 40.44

Lack of genotype and AMPH withdrawal effects on anxiety (for details, see Materials and Methods). Data are shown as mean $\pm$ SEM; $n = 7–8$ per group.

Table 3. Effects on sociability and social novelty after AMPH treatment

Test/parameter		$K_v10.1^{+/+}$	$K_v10.1^{-/-}$	$K_v10.1^{+/+}$AMPH	$K_v10.1^{-/-}$ AMPH
Sociability			Within 6 days after AMPH withdrawal		
Proximal contact (s)	Social side	113.06 ± 18.38	97.23 ± 15.97	100.80 ± 18.12	134.99 ± 22.08
	Empty side	65.54 ± 12.09	74.71 ± 14.10	72.35 ± 21.36	56.61 ± 17.82
Social novelty			Within 6 days after AMPH withdrawal		
Proximal contact (s)	Novel	72.30 ± 13.64	69.09 ± 11.68	72.50 ± 8.27	81.80 ± 12.90
	Familiar	51.98 ± 5.52	45.54 ± 5.88	61.86 ± 8.23	78.46 ± 13.64

Lack of genotype and AMPH withdrawal effects on sociability and social novelty preference measured in the three chamber apparatus (for details, see Materials and Methods). Data are shown as mean $\pm$ SEM; $n = 7–8$ per group.

decreased circadian locomotor activity [Fig. 5A; $F(1,27) = 8.85$, $P < 0.01$] and 23 h sucrose solution consumption [Fig. 5B; $F(1,27) = 15.74$, $P < 0.001$] in both genotypes. No effects of genotype were found in those tests except a significant group × circadian phase interaction [$F(1,3592) = 26.90$, $P < 0.0001$] with $K_v10.1^{-/-}$ mice being more active than $K_v10.1^{+/+}$ during the night (*post hoc* test $P < 0.0001$), but not the day phase.

Long-term effects of AMPH withdrawal in $K_v10.1^{-/-}$ mice
Starting 3 weeks after AMPH withdrawal, circadian activity, 23 h sucrose solution consumption (Fig. 5D), anxiety (Table 2, the elevated plus maze test and hyponeophagia),

learning and memory (Table 4, Y maze spatial novelty test, T maze spontaneous alternations test and fear conditioning) and sensorimotor gating (Table 5) were measured. No between genotype differences and no interactions with AMPH sensitization status were found in those tests except for circadian activity. Equivalent increases in activity were found in animals exposed to the drug irrespectively of genotype [Fig. 5C; $F(1,27) = 11.70$, $P < 0.01$], and a significant genotype × circadian phase interaction was found [$F(1,3592) = 6.82$, $P < 0.01$] with $K_v10.1^{-/-}$ mice highly significantly more active than $K_v10.1^{+/+}$ during the night (*post hoc*, $P < 0.0001$), but only slightly during the day phase ($P = 0.05$).
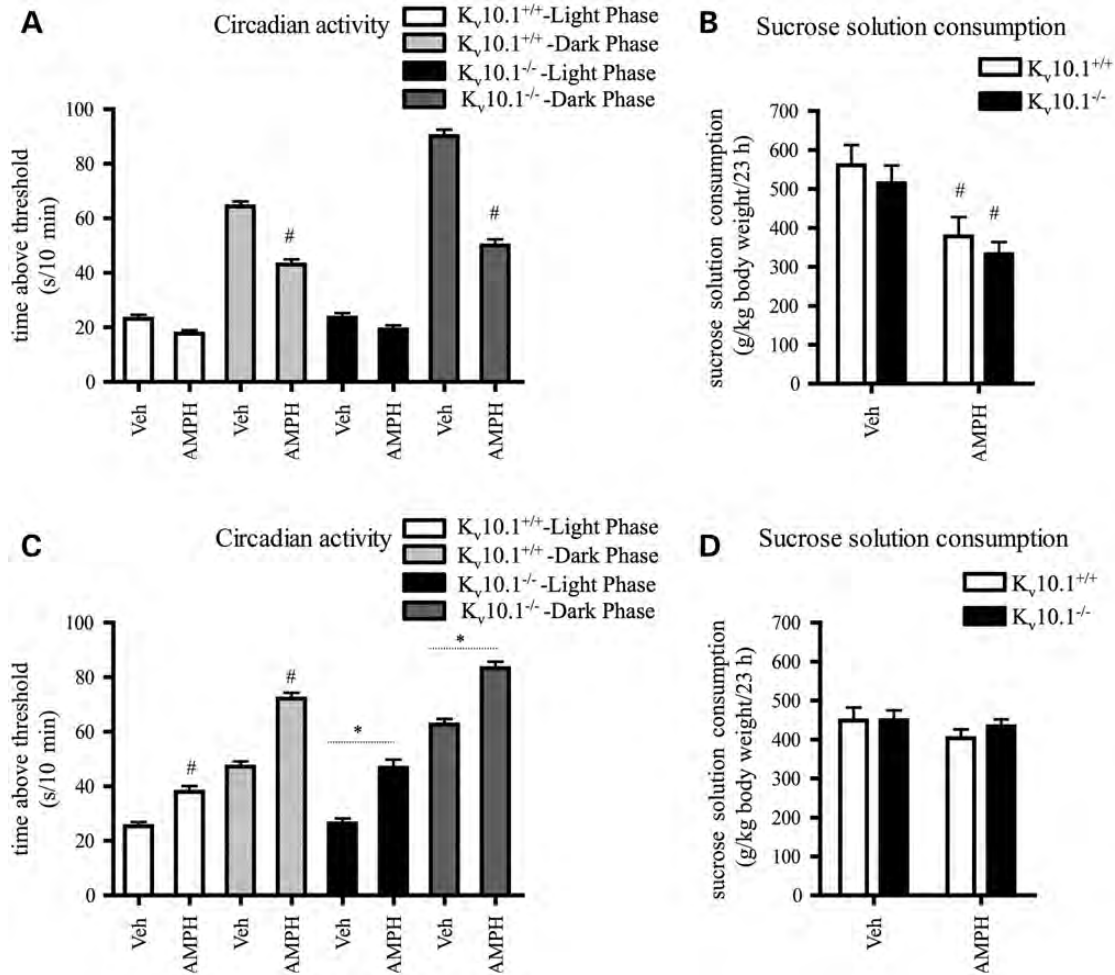
Figure 5. Genotype independent short-term (**A** and **B**) and long-term (**C** and **D**) effects of AMPH withdrawal on circadian activity and 23 h 4% sucrose solution consumption (for details, see Materials and Methods). Data are shown as mean + SEM; n = 7–8 per group. $^*P < 0.05$ versus $K_v10.1^{+/+}$, $^\# P < 0.05$ versus non-sensitized group (Veh).

Table 4. Learning and memory

Test/parameter	$K_v10.1^{+/+}$	$K_v10.1^{-/-}$	$K_v10.1^{+/+}$ AMPH	$K_v10.1^{-/-}$ AMPH
Y maze spatial novelty				
Time in novel arm (%)	54.98 ± 4.76	55.61 ± 4.41	49.53 ± 3.32	54.86 ± 2.67
Entries to novel arm (%)	46.16 ± 9.07	47.46 ± 11.11	42.76 ± 2.51	46.65 ± 1.50
T maze spontaneous alternations				
Accuracy after 1 min	0.93 ± 0.06	0.81 ± 0.09	0.93 ± 0.06	0.92 ± 0.07
Accuracy after 15 min	0.81 ± 0.09	0.87 ± 0.08	0.93 ± 0.06	0.92 ± 0.07
Accuracy after 30 min	0.62 ± 0.12	0.56 ± 0.14	0.56 ± 0.11	0.64 ± 0.14

Lack of genotype and AMPH withdrawal effects on learning and memory (for details, see Materials and Methods). Data are shown as mean ± SEM; $n = 7–8$ per group.
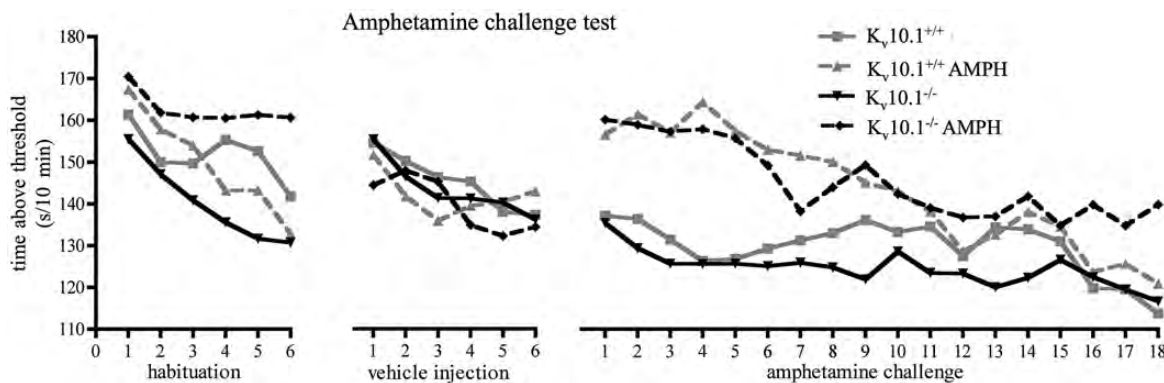
AMPH challenge

There were no significant differences in activity due to genotype or AMPH sensitization status during an initial 60 min habituation session [$F(1,27) = 0.00$, n.s. and $F(1,27) = 1.79$, n.s., respectively] or during the 60 min after vehicle injection [$F(1,27) = 0.48$, n.s. and $F(1,27) = 0.33$, n.s., respectively]. AMPH injection (1 mg/kg) increased activity to a higher degree in AMPH-sensitized animals [Fig. 6, $F(1,27) = 33.02$, $P < 0.0001$] and a significant interaction between AMPH sensitization status × within session period [$F(17,459) = 2.93$, $P < 0.0001$] was found, with $K_v10.1^{-/-}$ AMPH mice more active than $K_v10.1^{+/+}$ AMPH during the last 30 min of the test.

Table 5. Effects in auditory prepulse inhibition test after AMPH treatment

Prepulse inhibition (%)	$K_v10.1^{+/+}$	$K_v10.1^{-/-}$	$K_v10.1^{+/+}$ AMPH	$K_v10.1^{-/-}$ AMPH
Prepulse intensity		4 months after AMPH withdrawal		
4 dB above background (65 dB)	31.60 ± 3.85	19.08 ± 4.66	29.73 ± 4.96	31.81 ± 7.58
8 dB above background	61.24 ± 3.22	39.33 ± 9.03	50.95 ± 4.19	54.92 ± 5.89
12 dB above background	69.97 ± 3.54	58.28 ± 5.13	68.71 ± 3.28	63.86 ± 4.06
16 dB above background	81.04 ± 2.22	56.65 ± 5.53	80.81 ± 1.64	71.58 ± 3.67

Lack of genotype and AMPH withdrawal effects in auditory prepulse inhibition test (for details, see Materials and Methods). Data are shown as mean $\pm$ SEM; $n = 7-8$ per group.

Figure 6. Genotype independent increased activity in AMPH-sensitized mice during AMPH challenge test (1 mg/kg, i.p.) conducted 5 months after sensitization (for details, see Materials and Methods). Data are shown as mean; $n = 7-8$ per group.

Sensorimotor gating modified by apomorphine and haloperidol

There were no significant differences due to genotype [$F(1,27) = 2.34$, n.s.] or AMPH sensitization status [$F(1,27) = 1.21$, n.s.] in the prepulse inhibition test. There was a significant genotype-independent difference between the inhibition induced by different prepulse intensities [$F(2,2157) = 64.05$, $P < 0.0001$] and drugs used [$F(3,2157) = 52.40$, $P < 0.0001$], with haloperidol treatment reversing the decrease in prepulse inhibition induced by apomorphine (Fig. 7A; *post hoc* tests, $P < 0.0001$). There was also a statistically significant interaction between genotype × AMPH sensitization status × drug [$F(3,2157) = 10.95$, $P < 0.0001$] with $K_v10.1^{-/-}$ AMPH-sensitized mice showing increased reactivity to apomorphine (*post hoc* $P < 0.0001$) when compared with all other groups (Fig. 7B). There were no other significant interactions in this test.

Haloperidol-induced catalepsy modified by antidepressants

There was a significant difference between genotypes in the duration of haloperidol-induced catalepsy [Fig. 8; $F(1,27) = 5496.73$, $P < 0.0001$] with $K_v10.1^{-/-}$ mice showing longer latency to move. Imipramine and sertraline, but not fluoxetine, decreased haloperidol-induced catalepsy in both genotypes [main effect $F(3,297) = 385.82$, $P < 0.0001$; *post hoc* tests at least $P < 0.04$]. Statistically significant interactions between genotype × drug [$F(3,297) = 79.30$, $P < 0.0001$] and genotype × trial [$F(2,297) = 398.23$, $P < 0.0001$] were

driven by an increased reactivity to haloperidol in the $K_v10.1^{-/-}$ group. AMPH sensitization had no effect on haloperidol-induced catalepsy, regardless of genotype [$F(1,27) = 0.04$, n.s.].

DISCUSSION

$K_v10.1$ channels are delayed rectifier potassium channels widely expressed in the central nervous system (25,26). In *Drosophila*, they are involved in regulating excitability of the neuromuscular junction (36). Because in mammals no physiological function has been reported so far, we generated $K_v10.1$-deficient mice to elucidate the functional role of $K_v10.1$ in the brain. Successfully generated $K_v10.1$-deficient mice displayed no obvious differences from their littermate controls in the average life span, reproductive characteristics or development. Deletion of $K_v10.1$ did not lead to any gross anatomical or histological changes in the brain. Cortex, hippocampus and cerebellum using Nissl neuronal staining and neuronal markers such as NeuN, calbindin and calretinin did not show any morphological difference between both genotypes. Electrical properties of $K_v10.1$ in cerebellar PCs of $K_v10.1$-deficient mice were determined to elucidate the role of $K_v10.1$ in controlling firing and excitability without interference of $K_v10.2$ that is not expressed in PCs (8,25,28), although we had determined that $K_v10.2$ expression did not increase in $K_v10.1$-deficient mice using real time RT-PCR.
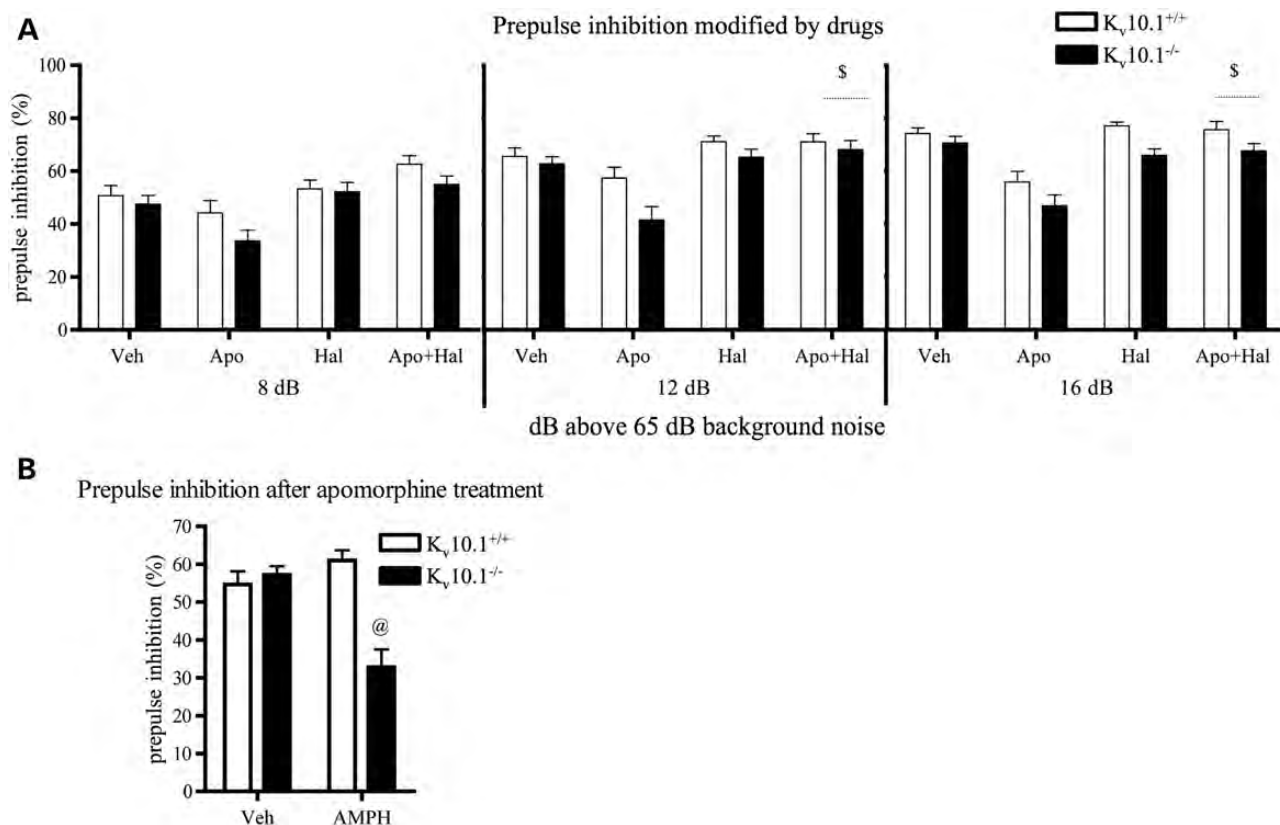
Figure 7. Genotype independent reversal of apomorphine (Apo, 2 mg/kg)-induced decrease in prepulse inhibition by haloperidol (Hal, 0.4 mg/kg) treatment (**A**, for details, see Materials and Methods). Observed increased reactivity to apomorphine in $K_v10.1^{-/-}$ mice was driven by highly significant increase in reactivity to Apo in $K_v10.1^{-/-}$ AMPH group (**B**, mean for all prepulse intensities). Data are shown as mean + SEM; $n = 5-16$ (A) and $7-8$ (B) per group. $\$P < 0.0001$ versus Apo, @$P < 0.0001$ versus all the other groups.
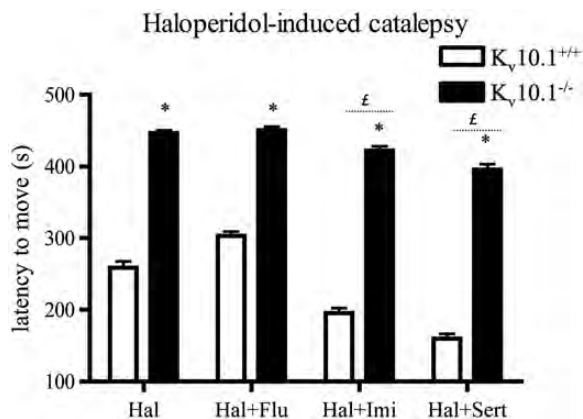

Figure 8. Haloperidol-induced catalepsy. Increased immobility, but normal reactivity to antidepressants in $K_v10.1^{-/-}$ mice in haloperidol-induced catalepsy test (for details, see Materials and Methods). Data are shown as mean + SEM; $n = 15-16$ per group. £$P < 0.01$ versus Hal, *$P < 0.0001$ versus $K_v10.1+/+$. Hal, haloperidol (1 mg/kg); Imi, imipramine (20 mg/kg), Flu, fluoxetine (20 mg/kg), Sert, sertraline (5 mg/kg). Data from AMPH-sensitized and non-sensitized animals were pooled due to a lack of differences.

We measured a slight increase in input resistance in $K_v10.1^{-/-}$ cells that is, however, not reflected in an earlier onset of firing or in an increased firing frequency after crossing the threshold. $K_v10.1$, thus, could still be involved in setting the membrane potential in PCs, but its contribution is relatively small. We could not detect any difference between both genotypes in membrane potential, firing frequency and action potential shape of cerebellar PCs. We can, therefore, speculate that the previously strong staining for $K_v10.1$ in the PC soma (26) results from a synaptic expression in the terminals of climbing fibres or basket cells, with only a minor expression in the PC itself. This actually would be in line with *in situ* hybridization data published by Saganich *et al*. (25) that showed a strong expression of $K_v10.1$ mRNA in the granule layer, but not in the PCs.

Although $K_v10.1$ is only expressed in the brain, the absence of $K_v10.1$ expression in $K_v10.1$-deficient mice does not cause any substantial physiological problems, indicating that $K_v10.1$ function is not crucial for mice life. However, $K_v10.1$ is essential for zebrafish development and patterning indicating early mortality and cell detachment in $K_v10.1$ knockdown zebrafish (37). This difference may be attributed to evolutionary differences, similarly to caveolin-1, the deletion of which is only lethal in zebrafish, but not in mice (38).

At the behavioural level, $K_v10.1^{-/-}$ mice manifest only hyperactivity both during 60 and 23 h of spontaneous activity sessions. All other tests applied measuring general health, sensorimotor functioning and gating, anxiety, social behaviour, learning and memory indicated comparable results in both genotypes. AMPH sensitization used as a standard procedure

to induce schizophrenic-like aberrations in rodents (39,40) did not differentiate between $K_v10.1^{-/-}$ and $K_v10.1^{+/+}$ animals, except that $K_v10.1^{-/-}$ AMPH-sensitized mice display an increased reactivity to apomorphine in the prepulse inhibition test. This might suggest hyperreactivity of the dopaminergic system in these animals or, consistent with our haloperidol-induced catalepsy test results, point to a decreased density/number of dopaminergic receptors.

As reported in previous studies (for review, see 41), AMPH withdrawal after sensitization procedure induces a depression-like state in mice lasting several days, characterized by a significant decrease in locomotor activity and sucrose consumption, but has no impact on anxiety or social behaviour. Three weeks after AMPH withdrawal, locomotor activity was significantly higher in AMPH-sensitized animals, but sucrose consumption returned to the level observed in non-sensitized animals.

Haloperidol reversed the apomorphine-induced decrease in prepulse inhibition and, as reported earlier (42), increased baseline PPI in sensorimotor gating test in all groups of animals. In contrast to some previous reports (for discussion, see 43), AMPH withdrawal did not induce decrease in the inhibition in our mice. A highly significant increase in responsiveness to haloperidol was found in the $K_v10.1^{-/-}$ group in the haloperidol-induced catalepsy test, which has been suggested as an experimental model of parkinsonism (44), irrespective of whether or not there had been AMPH sensitization. Haloperidol blocks dopaminergic receptors, especially D2 receptors, in the mesocortex and the limbic system of the brain and is effective in the treatment of acute psychotic states (45); however, by blocking the dopaminergic action in the nigrostriatal pathways, haloperidol induces extrapyramidal-motoric side effects such as dystonias, akathisia and pseudoparkinsonism (46). The hyperresponsivity to cataleptic effects of haloperidol that we have now observed in $K_v10.1^{-/-}$ mice may suggest a decreased density/number of somatodendritic D2 receptors in these mice (47,48). It, therefore, seems possible that a combination of lower doses of haloperidol and $K_v10.1$ agonists might prove to decrease the side effects without reducing the potent antipsychotic activity of haloperidol. These interesting findings, combined with the colocalization of $K_v10.1$ and tyrosine hydroxylase-positive dopaminergic neurons in the midbrain (49), suggest that $K_v10.1$ may be related to or influence the dopaminergic system. This possibility merits further study.

Overall, our behavioural tests did not show any signs of schizophrenic-like aberrations in $K_v10.1^{-/-}$ mice and revealed an almost complete lack of behavioural changes, except for mildly increased activity. This pattern of outcomes may prove to have important clinical implications in a rather different domain. $K_v10.1$ expression has been shown to be correlated with early cancer development of many tumours. In addition, $K_v10.1$ favours tumour progression (15). Therefore, shutting down $K_v10.1$ function has been proposed as a potential strategy to treat cancer (50–52). However, this approach necessitates an evaluation of the consequences induced by $K_v10.1$ deletion. The fact that abolition of channel function does not result in serious cognitive and/or behavioural effects speaks in favour of the feasibility of cancer treatments aimed against this newly validated tumour target.

MATERIALS AND METHODS

Generation of $K_v10.1^{-/-}$ mice

Targeting vectors were constructed to generate a deletion of exon 7 that encodes amino acid residues 344–388 of the $K_v10.1$ peptide. Genomic regions used in construction of the targeting vector were cloned from a 129/Sv mouse genomic library in λfixII (Stratagene). A 7.7 kb BstEII/SalI fragment from intron 6 was cloned into pBluescript-LoxPneoLoxP vector as the 5′ arm. A Nhe/Nsi fragment was used to generate a 2.25 kb 3′arm from intron 7 that was ligated into pBluescript-Exon-Lox. The mK$_v$10.1 targeting vector was constructed by the simultaneous ligation of the following four fragments: a 9.6 kb XhoI/SalI fragment containing the previously ligated 7.7 kb 5′ arm and the pBluescript-V2-TK cassette, a 2.2 kb Nhe/Nsi fragment that constitutes the 3′ arm, a 1.6 kb SalI/Nhe fragment containing an Exon 7 and a LoxP site. The resulting 18.4 kb targeting vector was linearized with *Hin*dIII and electroporated into 129/SvJ ES cells. Resistant cells were selected in the presence of G418 and ganciclovir as described previously. A total of 200 clones were picked, and DNA was isolated (at Genoway). A 0.4 kb fragment generated from the sequence immediately upstream of the 3′ arm was used to screen ES cell genomic DNA for correct homologous recombination by Southern Blot (Fig. 1). One ES cell was positive for homologous recombination and was injected into C57BL/6 blastocysts that were subsequently transferred into pseudo-pregnant females to generate chimeric offspring. Chimeras were bred with C57BL/6 females to generate heterozygotes. Germline transmission was determined by a combination of colour and genotyping.

Adult *Ella*Cre transgenic mice were bred with 8-week-old $K_v10.1^{NeoLoxP}$ (F0 crossing) mice. Offspring (F1) were screened for the presence of *Ella*Cre by PCR. Partial (flox) or complete (null) Cre recombination patterns were analysed by PCR. All analyses were carried out on null allele.

Mice were housed in a 12 h light–dark cycle facility with free access to food and water. Morphological and electrophysiological experiments were carried out in accordance with German laws governing the use of laboratory animals. Behavioural testing was conducted in accordance with the UK Animals (Scientific Procedures) Act 1986.

Genotyping of mutant mice

Routine genotyping of mice was performed by PCR on DNA isolated from tail biopsies. Briefly, tail samples were incubated at 56°C (2 h or overnight) in lysis buffer (100 mM Tris pH 8.5, 5 mM EDTA pH 8.0, 200 mM NaCl, 0.2% sodium dodecyl sulphate and 0.1 mg/ml proteinase K), followed by isopropanol precipitation. The DNA was pelleted by centrifugation, washed with 70% ethanol and resuspended in 100 μl H_2O. For genotyping of $K_v10.1^{neoloxP}$ knockouts, four primers were used: (5′F, 5′-TGCGTACATGGTGCTT GATTTC-3′, NeoR 5′-CGCGAAGGGGCCACCAAAG-3′, ExF, 5′-CATGATGATTGGCTGTGAGTATG-3′ and 3′R, 5′-CCCTCTTTCCACTAACAGCATC-3′), which resulted in products of 480 bp for the wild-type gene and 503 bp for the presence of the neomycin resistance cassette, 534 bp for the null allele and 580 bp for the flox allele. The four primers

were used in a multiplex PCR with Biotherm Polymerase (Genecraft) with the following amplification conditions: at 95°C for 4 and 30 cycles at 95°C for 30 s, 60°C for 30 s, 72°C for 50 s and a 7 min incubation at 72°C at the end of the run. Amplification products were resolved on a 1.5% agarose gel. For genotyping of the presence of *Ella*Cre, two primers were used (Cre-F, 5′-TCGATGCAACGAGTGA TGAG-3′ and Cre-R, 5′TTCGGCTATACGTAACAG-3′) with Biotherm Polymerase (Genecraft) with the following amplification conditions: at 95°C for 4 min, 30 cycles at 95°C for 10 s, 55°C for 20 s, 72°C for 10 s and a 7 min incubation at 72°C at the end of the run. For null allele genotyping, only 5′F, ExF and 3′R Primer were used.

Real time RT-PCR

Mice were sacrificed by CO_2 inhalation followed by decapitation. Brains were removed and different brain regions dissected. The tissue was washed in ice cold phosphate-buffered saline (PBS) and stored in RNAlater buffer (Applied Biosystems, Foster City, USA) at −20°C. Five micrograms of total RNA was obtained from brain tissues using the RNAeasy mini kit (Qiagen, Hilden, Germany), and first strand cDNA was produced using SuperScript (Invitrogen, Karlsruhe, Germany) with oligo dT. A housekeeping gene, Transferrin receptor (TfRc), was used as a control for RNA integrity and quantification. Real time RT-PCR was performed in triplicates on 100 ng cDNA using the Light Cycler Detector (Roche). The following fragments were amplified: 1079−1138 nt from sequence NM_001038607 detected with the mK_v10.1a probe [5′-(FAM)-AACAGGCTGCTGATGCCCTCATCCAC-(TAMRA)-3′]; 1528−1628 nt from sequence NM_011638 detected with the mTfRc probe [5′-(JOE)-ACTGAGTGGT TGGAGGGATACCTTTCATCT-(TAMRA)-3′]; 2320−2429 nt from sequence NM_172805 detected with the mK_v10.2 probe [5′ (FAM)-GATGGAGAGGACCTTCTCTGTGTCG-(6-TAMRA)-3′]. Conditions for the PCR reaction were as follows: 50°C for 2 min; 95°C for 10 min; 95°C for 15 s, 56°C for 15 s and 60°C for 1 min (40 cycles). The number of PCR cycles to reach detection threshold was used to determine specific mRNA content with a standard curve for interpolation.

Immunohistochemistry

Mice were anaesthetized with ketamine (75 mg/kg, Medistar, Holzwickede) and xylazine (15 mg/kg, Riemser, Greifswald) and subsequently transcardially perfused with PBS pH 7.4 and then with 4% paraformaldehyde (Sigma). Paraffin embedding was done as previously described (26). Brains were serially cut in the sagittal plane at 5 μm thicknesses with a microtome (Model RM2255, Leica, Berlin, Germany) and collected on superfrost-coated slides (Thermo Scientific). The plane of sectioning was oriented to match the drawings of the mouse brain atlas. Brain morphology was analysed by using Nissl staining (53). For immunohistochemistry, paraffin sections were stained with specific markers using Discovery XT staining module (Ventana Medical Systems, Roche). Primary antibodies, including NeuN (1:900, Chemicon), Calbindin (1:1000, Millipore) and Carletinin (1:1000, Chemicon)

were incubated for 1 h at 37°C, followed by incubation for 32 min at room temperature with biotinylated secondary antibodies (Vector Labs). Immunostaining was developed using streptavidin-peroxidase and 3,3′-diaminobenzidine and counterstained with haematoxylin. Images were obtained with an Axioskop microscope (Zeiss, Goettingen, Germany) equipped with a digital camera (Micropublisher 5.0, QImaging Surrey, Canada). Linear contrast and brightness corrections were performed using Adobe Photoshop.

Electron microscopy

K_v10.1$^{+/+}$ and K_v10.1$^{-/-}$ mice, 8 weeks old, were anaesthetized and perfused transcardially with Hank's balanced salt solution, followed by fixation in 4% paraformaldehyde (Serva, Heidelberg, Germany) and 0.2% glutaraldehyde (EM grade, Science Services, München, Germany) in 0.1 M phosphate buffer pH 7.3. After dissection, slices of the cerebellar vermis were postfixed with 2% OsO_4 (Science Services, Munich, Germany) in 0.1 M phosphate buffer pH 7.3 and embedded in EPON (Serva) after dehydration with ethanol and propylene oxide. Ultrathin sections were prepared with a Leica Ultracut S ultramicrotome (Leica, Vienna, Austria), stained with an aqueous solution of 4% uranyl acetate, followed by lead citrate (Reynolds, 1963). EM pictures were taken with a LEO 912 AB electron microscope (Zeiss, Oberkochen, Germany) using an on-axis 2k CCD camera (TRS, Moorenweis, Germany).

Speed congenics

To generate a congenic C57Bl6/N strain, marker-assisted selection of breeders (Elchrom Scientific) was used, and the progeny containing the highest percentage of C57Bl6/N was selected for further backcrossing. Seven backcrossings were needed to obtain 99.9% C57Bl6/N.

Whole-cell current-clamp recordings on cerebellar PCs

K_v10.1$^{+/+}$ and K_v10.1$^{-/-}$ littermates aged 20−28 days were decapitated under isoflurane anaesthesia. The cerebellum was removed and placed in an ice-cold solution containing (in mM) 60 NaCl, 120 sucrose, 25 $NaHCO_3$, 1.25 NaH_2PO_4, 2.5 KCl, 25 D-glucose, 0.1 $CaCl_2$, 3 $MgCl_2$, 3 myo-inositol, 2 sodium pyruvate and 0.4 ascorbic acid. Coronal slices of the cerebellar vermis were cut using a Leica VT1200S vibratome. The slices were kept at 36°C for 1 h in artificial cerebrospinal fluid containing (in mM) 125 NaCl, 2.5 KCl, 25$NaHCO_3$, 1.25 NaH_2PO_4, 2 $CaCl_2$, 1 $MgCl_2$, 3 myo-inositol, 2 sodium pyruvate and 0.4 ascorbic acid that was continuously bubbled with 95% O_2 and 5% CO_2. For measurements, slices were transferred to a recording chamber and constantly perfused with artificial cerebrospinal fluid at 2−3 ml/min. The bath temperature was maintained at 33 ± 1°C with an in-line solution heater (Warner instruments). All recordings were performed in the presence of the GABA$_A$-receptor antagonist SR95531 [2-(3-carboxypropyl)-3-amino-6-(4-methoxyphenyl) pyridazinium bromide] and the AMPA-receptor antagonist NBQX [2,3-dihydroxy-6-nitro-7-sulfamoyl-benzo(f)quinoxaline-2,3-dione] (Tocris).

Thick-walled borosilicate pipettes were pulled to resistances of $3-4\,M\Omega$ and filled with intracellular solution containing (in mM) 135 K-gluconate, 10 KCl, 10 HEPES, 5 MgATP, 0.5 NaGTP and 0.1 EGTA. Whole-cell current-clamp recordings were performed with an EPC 10/2 amplifier controlled by Patchmaster software (Heka) using difference interference contrast optics on a Zeiss Axioskop. A calculated liquid junction potential of 14 mV was subtracted from the recorded voltages. Data were filtered at 10 kHz and sampled at 100 kHz. Offline analysis was done using Igor Pro software (Wavemetrics) with custom written macros and the Neuromatic software package (ThinkRandom). Statistics were performed with Prism software (GraphPad). Data are presented as mean $\pm$ SEM.

Behavioural experiments

For behavioural testing, adult female mice ($11-12$ weeks at the beginning of experiments) were used. All animals were group housed with *ad libitum* access to water and food pellets, under a 12 h light/dark cycle, in controlled constant temperature ($21 \pm 2°C$) and humidity (60%). All experiments were conducted during the light phase from 9 a.m. to 5 p.m.

Procedure

The behavioural part of the present study had four stages. The first stage involved general health screening and basic sensorimotor test battery, spontaneous locomotor activity and motor coordination measured by rotarod test. The second phase started with AMPH sensitization, followed by circadian activity, sucrose consumption, social interaction and light/dark box test conducted within 6 days after AMPH withdrawal to measure the depressive-like state induced by the termination of AMPH treatment. The third stage started 3 weeks after AMPH withdrawal and included circadian activity, sucrose consumption, the elevated plus maze test, hyponeophagia test, T maze spontaneous alternation and the Y maze test, prepulse inhibition, startle reaction habituation, fear conditioning and finished with an AMPH challenge test 5 months after AMPH sensitization. The fourth stage started 3 weeks after the AMPH challenge test and involved apomorphine-induced decrease in prepulse inhibition and its reversal by haloperidol and haloperidol-induced catalepsy and its modification by antidepressants (imipramine, fluoxetine and sertraline).

General health screening and basic sensorimotor test battery

Procedures were based on previously published protocols (54) with some modifications. Single animals were observed in a transparent plastic cage [17 cm (d) $\times$ 27 cm (w) $\times$ 20 cm (h)] for 3 min for any signs of stereotypy, convulsions, excessive activity, tremor, freezing and grooming. Coat condition, including bald patches and piloerection, missing whiskers and presence of any physical abnormalities were scored by direct inspection. Motor abilities and motor reflexes were scored by: (i) trunk curl: the mouse was held up by its tail, which elicits a clearly observable forward curling of its abdomen, (ii) forepaw reaching: forepaw reaching movements

in the mouse held suspended by the tail and slowly moved towards a metal rod, (iii) inverted screen: the mouse was placed in the centre of a screen (20.5 cm $\times$ 13 cm-wire mesh, 12 mm^2 holes) and the screen was inverted over a 2 s period with the mouse's head declining and held steadily 90 cm above a solid, cushioned surface; latency to falling was noted, with a cutoff time at 60 s and (iv) reactivity to handling, scored as follows: 1—the mouse struggles when held by its tail, 2—the mouse struggles when held by the neck, 3—the mouse struggles when lying supine and 4—no struggle; test was terminated at any point when struggling was apparent; pinna reflex and whisker twitch: the mouse was placed on to a grid and the proximal part of the inner canthus and the whisker were touched lightly with the tip of a cotton probe (ear retraction and whisker reaction: absent/present). Olfaction was measured in a separated 3 min test: the mouse was placed in a plastic transparent cage [17 cm (d) $\times$ 28 cm (w) $\times$ 17 cm (h)] with a drop of diluted (1:100) almond oil (Langdale, England) on the wall 4 cm from the floor. Sniffing time, number of sniffs and latency to the first sniff were scored using the AnyMaze system (Stoelting, USA).

AMPH sensitization

D-amphetamine sulphate (Sigma Chemical Co., St. Louis, MO, USA) was dissolved in a 0.9% NaCl solution to obtain the required concentrations. All the solutions were freshly prepared and administered in a volume of 5 ml/kg. Mice were weighed each day and injected intraperitoneally every 6 h with increasing doses of AMPH ($1-2-3$ mg/kg on day 1, $4-5-6$ mg/kg on day 2, $7-8-9$ mg/kg on day 3 and 10 mg/kg on day 4 once only). Control animals were given physiological saline injections.

AMPH challenge

Five months after AMPH sensitization, animals were subjected to the AMPH challenge test. The Threshold system (Version 3, Med Associates) converting change in pressure on plates into changes in voltage was used. Mice were placed in cages of 22.5 $\times$ 12.5 $\times$ 13 cm. The lower detection threshold was set to 20 V and the upper threshold to 50 V. The time spent between the two threshold values was taken to represent locomotor activity in the mice and was collected in 10 min time bins over three consecutive phases: a 60 min initial habituation followed by saline injection and 60 min free exploration, and the third stage, 180 min of free exploration after intraperitoneal injection with 1 mg/kg AMPH.

Locomotor activity

Open field
Spontaneous activity was analysed using automated activity chambers (27.3×27.3 cm) with 3 16 beam I/R arrays (ENV-510, MED Associates Inc., St. Albans, VT, USA). Horizontal and vertical activity (rearing), mobility and immobility time, total distance (cm) and velocity (cm/s) were automatically scored. Data were collected in 5 min intervals over a 60 min test session.

Circadian activity

The Threshold system (Version 3, Med Associates) converting changes in pressure on plates into changes in voltage was used to measure the circadian cycle activity of mice over a 23 h period (8 a.m. till 7 a.m. the next day). Mice were placed in cages of $22.5 \times 12.5 \times 13$cm and left with *ad libitum* food and water. The time spent above 20 V threshold was taken to represent locomotor activity in the mice and was collected in 1 h time bins. The first 3.5 h of data were not included in the analysis, as this largely represents habituation to the apparatus. Circadian activity was assessed three times: (i) within 5 days after AMPH withdrawal and (ii) 3 weeks after AMPH withdrawal with activity scoring accompanied by 23 h two bottle free-choice sucrose (4%) preference test and (iii) 5 months after AMPH withdrawal during AMPH challenge test.

Motor coordination

Accelerating rotarod

Quantitative measurements of motor coordination were performed using an accelerating rotarod (Model 7650, Ugo Basile, Comerio, VA, Italy) according to the previously published protocol (55). Mice were placed on a rod moving at 4 rpm that, after 10 s, began to accelerate at a rate of 20 rpm/min. Mice were given two trials per session and three sessions per day with a 2 h intersession interval. Mean speed at fall from two consecutive runs was used as a measure of motor coordination and motor learning.

Social behaviour

Social approach task: habituation, sociability phase and preference for social novelty phase

Social approach behaviours were tested in a modified three-chambered apparatus based on methods previously described (56). The apparatus was a rectangular, three-chambered box made of red-tinted Plexiglas (inner compartments size: 20 cm $\times 30$ cm). Manually retractable horizontal doorways built into the two dividing walls (15 cm high) controlled access to the side chambers through a 10 cm passage. A top mounted digital video camera (Ikegami Tsushinki, Japan) was placed over the boxes to record the session. Stimulus mice (male CD1) were habituated to the apparatus and to the wire cage enclosure ($8.1 \times 8.1 \times 21.8$ cm), several days before the start of experiments. The test session began with a 10 min habituation to all three chambers, during which lack of innate side preference was confirmed. The subject was then briefly confined to the centre chamber, whereas the steel wire cage described above was placed in one of the side chambers. A novel stimulus CD1 mouse was placed in an identical wire cage located in the other side of the chamber. The side containing the novel object and the novel mouse alternated between the left and right chambers across subjects. After both stimuli were positioned, the two side doors were simultaneously removed, and the subject was allowed access to all three chambers for 10 min. Next, the mouse was again restricted to the central chamber, and the empty wire cage replaced by a new one containing a new stimulus animal. The subject was then allowed access to all

three chambers for 10 min. Time spent in proximity (2 cm) to the wire cages was recorded and analysed by an AnyMaze video tracking system (Stoelting, USA). The apparatus and wire cages were cleaned with water and 70% alcohol, respectively, between subjects.

Anxiety

Elevated plus maze

The elevated plus maze test was performed as described by Lister (57), with some modifications. The plus maze constructed from opaque polyvinyl plastic consisted of two open arms (27×5 cm) with a low (0.2 cm) edge and two closed arms (27×5 cm) with 30 cm walls connected to a central zone (5×5 cm) to form a cross, illuminated by a ceiling lamp (30 lux at the level of the maze). It was elevated to a height of 50 cm from the floor. The mouse was placed on the central zone facing one of the open arms. An arm entry was scored when the mouse placed all four paws into the arm, and an arm exit when all four paws were removed. The maze floor was cleaned thoroughly between trials using water. The time spent in the open arms and number of open arms entries were recorded for a 5 min period using the AnyMaze system (Stoelting, USA). Anxiety measures were calculated using the following formula: percentage of time spent in the open arm = time spent in the open arms/(the sum of time spent in both classes of arms) $\times$ 100; percentage of open arm entries = (number of entries in the open arms/total number of entries) $\times$ 100.

Light/dark box

The light/dark box test was performed as previously described (58). Med Associates activity chambers (ENV-510) were used. The dark box insert was made of black Perspex designed to cover half of the area of the activity chamber ($27 \times 13.9 \times 21.5$ cm) with a 4×4 cm hole placed in the middle of the wall at floor level. Time spent in and latency to enter light and dark zones as well as the number of full-body transitions between the light (300 lux) and dark (2 lux) compartments were automatically scored by Med Associates activity software. The mouse began the experiment in the light compartment.

Hyponeophagia

Hyponeophagia was tested as previously described (59). Sweet corn kernels were evenly distributed on a white Perspex base (30 cm^2) covered with a translucent plastic jug (approximate volume 1.5 l, 15 cm diameter) placed upside down. Tests were conducted under standard laboratory strip lights. Animals were food deprived overnight. Mice were singly housed for 20 min prior to testing. The latency to begin to eat (>2 s uninterrupted consumption) was recorded. Animals that failed to eat within the 120 s were re-tested 3 min later, for a maximum of three trials, and the sum of the latencies was noted.

Learning and memory

Spontaneous alternation

The apparatus consisted of a wooden black T maze. Each arm ($30 \times 10 \times 29$ cm) contained a thin layer of unfamiliar female

bedding. A removable central partition extended 7 cm from the back of the T into the start arm, dividing the choice area and allowing access to only one goal arm at a time. A mouse was placed in the start arm (stem of the 'T'), facing away from the goal arms and allowed to freely explore. After it had entered a goal arm, it was confined there for 30 s by closing a guillotine door, then following a delay of 1, 15 or 30 min, it was returned to the start arm with all doors raised. If the mouse chose to enter the same arm it had previously explored, this was recorded as an error. Each mouse received two trials with each delay over 3 days. Delays order was counterbalanced within group. The inter-trial interval was 3 h.

Y maze spatial novelty

This task was based on a previously published protocol (60). A Perspex Y maze with arms of $30 \times 8 \times 20$ cm was placed into a room containing a variety of extra-maze cues. A thin layer of wood chips covered the floor. This was not changed between mice, but was redistributed between phases for individual mice and between mice to eliminate meaningful intramaze cues. Mice were assigned two arms (a start arm and one other arm) to which they were exposed during the first trial, the exposure phase, for 5 min. This selection of arms was counterbalanced with respect to genotype. An entry/exit into/from an arm was defined by a mouse placing all four paws inside/outside an arm. The test phase began 1 min after the exposure phase, during which the mouse had been put into a holding cage. During the test phase, mice were allowed free access to all three arms. Mice were placed at the end of the start arm and allowed to explore all three arms for 2 min. The time that mice spent in each arm was recorded and analysed by AnyMaze system (Stoelting, USA). Novelty preference was calculated as time in novel arm $\times$ 100 (time in all three arms).

Fear conditioning

Fear-conditioning experiments were carried out by a computer-controlled fear-conditioning system (TSE-Systems, Bad Homburg, Germany) as previously described (61). During training, mice initially explored the context for 180 s. Thereafter, a single paired (delay) presentation occurred with a 30 s tone (5 kHz, pulsed 5 Hz and 70 dB SPL) followed at tone offset by a 1 s shock (unconditioned stimulus: US; 0.5 mA, constant current). The US was delivered through the stainless steel floor grid (4 mm, distance 9 mm) in the fear-conditioning box. Mice were returned to their home cages 30 s after US offset. Acquisition occurred in a transparent Plexiglas cage [36 cm (w) $\times$ 21 cm (d) $\times$ 20 cm (h)] placed within a fear-conditioning box that was made of white acrylic plastic, under a broadband auditory background noise (white noise, 50 dB SPL) and constant light (80 lux). The fear-conditioning cage was thoroughly cleaned with 70% ethanol before each experiment.

   Context-dependent memory was tested 24 h after acquisition by re-exposure to the conditioning box for 180 s without any phasic stimulation such as tone and shock. The tone-dependent (cued) memory test was performed 24 h after

the contextual memory test in a novel context. The novel context was a rectangular black Plexiglas box [36 cm (w) $\times$ 21 cm (d) $\times$ 20 cm (h)] with plain white frozen floor installed within TSE-activity photo beam system. The light intensity was reduced to 6 lux, and strawberry smell (Dale Air Ltd, UK) was introduced to render the novel context different from the conditioning context. Initially, behaviour was monitored for 180 s without tone presentation (pre-CS phase) before the tone was replayed for 180 s (CS phase). The last minute of the pre-CS phase and the first minute of the CS phase were used for assessment of cued-conditioned responses. Freezing time was calculated by the fear-conditioning system to determine shock and cued responses. The threshold for freezing was set at 2 s.

Prepulse inhibition of acoustic startle

Prepulse inhibition

Two months later, startle response and prepulse inhibition of acoustic startle responses were measured by the SR-Lab System (San Diego Instruments, San Diego, CA, USA). A test session began by placing a mouse in the Plexiglas cylinder, where it was left undisturbed for 5 min. A test session consisted of 10 trial types: a 40 ms, 120 dB sound burst used as the startle stimulus, 4 different acoustic 20 ms prepulse stimuli: 69, 73, 77, 81 dB (4, 8, 12 and 16 dB above the background noise) and 4 combinations of prepulses and startle stimuli spaced by 100 ms delay, starting with the onset of the prepulse stimulus. Finally, there were trials in which a 65 dB stimulus (identical to the background noise) was presented to measure baseline movement in the cylinders. Six blocks of the 10 trial types were presented in pseudorandom order such that each trial type was presented once within a block of 10 trials. The session started and finished with five startle stimuli. The average inter-trial interval was 15 s (ranged from 10 to 20 s). The average startle amplitude was recorded every 1 ms during the 65 ms sampling window starting at the onset of the startle stimulus in pulse-alone and prepulse-plus-pulse trials, and at the onset of the prepulse stimulus, the prepulse-alone trials were used to determine the stimulus reactivity. The following formula was used to calculate percentage of prepulse inhibition of a startle response: $100 - (\text{prepulse-plus-pulse} \times 100 / \text{pulse-alone})$.

Prepulse inhibition modified by apomorphine and haloperidol

Two months later, startle response and prepulse inhibition of acoustic startle response after apomorphine, haloperidol, apomorphine + haloperidol or vehicle (0.09% saline) were measured in a Latin square design using stimuli identical to the described above. Each animal was exposed to each solution once every 2 days. All drug solutions were freshly prepared on the day of testing and were administered in a volume of 10 ml/kg. Apomorphine HCl (Apo, Sigma Chemicals, St. Louis, USA) was dissolved by sonication in sterile 0.9% NaCl solution to obtain the required concentration of 2.0 mg/kg. Haloperidol (Hal, Janssen-Cilag, Baar, Switzerland) was prepared from solvent ampoules (5 mg/ml) diluted

with sterile 0.9% NaCl solution to obtain the required concentration of 0.4 mg/kg. The first injection (Hal or saline solution) was made 60 min before testing via the intraperitoneal route. The second injection, either Apo or saline solution, was administered 15 min before testing via the subcutaneous route. The doses and pretreatment times were based on those commonly employed in studies of a similar nature in mice (62). The first five startle-alone trials were excluded. The reactivity scores obtained on prepulse-plus-pulse trials and pulse-alone trials were converted into percentage score denoting the percentage of inhibition of startle response at each prepulse intensity by the formulae: 100−(prepulse-plus-pulse × 100/pulse-alone).

Haloperidol-induced catalepsy modified by antidepressants

Catalepsy was measured by the bar test. Mice were positioned so that their hindpaws were on the bench and their forelimbs rested on a 1 cm diameter horizontal metal bar, 4 cm above the bench. The length of time the mice maintained this position was recorded to a maximum of 600 s. Measurements were conducted 60, 120 and 180 min after haloperidol administration (1 mg/kg, intraperitoneally). The following drugs were administered intraperitoneally 30 min before haloperidol: imipramine (20 mg/kg), fluoxetine (20 mg/kg), sertraline (5 m g/kg) or saline (0.09%). Each animal was exposed to all drug solutions (Hal + Imi, Hal + Flu, Hal + Ser and Hal + Veh) every second day according to a Latin Square design.

Behavioural data analysis

Data were analysed using one- or two-factor analysis of variance (ANOVA), followed by Bonferroni-modified least significant difference tests. When animals were tested several times in the same task or when within-session periods were used, ANOVAs with repeated measures were applied. All tests of significance were performed at $\alpha = 0.05$ using Unistat 5.6 (Unistat Ltd, London, UK).

SUPPLEMENTARY MATERIAL

Supplementary material is available at *HMG* online.

ACKNOWLEDGEMENTS

We thank Johanna Widera and Bärbel Heidrich for excellent technical assistance.

Conflict of Interest statement: L.A.P. and W.S. are shareholders of iOnGen AG, a company developing K$_v$10.1 for diagnostic and therapeutic use.

FUNDING

This work was supported by the Max Planck Society (Tandem Grant). Funding to pay the Open Access publication charges for this article was provided by Max Planck Society.

REFERENCES

1. Warmke, J., Drysdale, R. and Ganetzky, B. (1991) A distinct potassium channel polypeptide encoded by the Drosophila eag locus. *Science (New York, N.Y.)*, **252**, 1560–1562.
2. Warmke, J.W. and Ganetzky, B. (1994) A family of potassium channel genes related to eag in Drosophila and mammals. *Proc. Natl. Acad. Sci. USA*, **91**, 3438–3442.
3. Bruggemann, A., Pardo, L.A., Stuhmer, W. and Pongs, O. (1993) Ether-a-go-go encodes a voltage-gated channel permeable to K+ and Ca2+ and modulated by cAMP. *Nature*, **365**, 445–448.
4. Kaplan, W.D. and Trout, W.E. 3rd. (1969) The behavior of four neurological mutants of Drosophila. *Genetics*, **61**, 399–409.
5. Pearson, G., Robinson, F., Beers, GT., Xu, B.E., Karandikar, M., Berman, K. and Cobb, M.H. (2001) Mitogen-activated protein (MAP) kinase pathways: regulation and physiological functions. *Endocr. Rev.*, **22**, 153–183.
6. Sutton, K.G., McRory, J.E., Guthrie, H., Murphy, T.H. and Snutch, T.P. (1999) P/Q-type calcium channels mediate the activity-dependent feedback of syntaxin-1A. *Nature*, **401**, 800–804.
7. Hegle, A.P., Marble, D.D. and Wilson, G.F. (2006) A voltage-driven switch for ion-independent signaling by ether-a-go-go K+ channels. *Proc. Natl. Acad. Sci. USA*, **103**, 2886–2891.
8. Ludwig, J., Weseloh, R., Karschin, C., Liu, Q., Netzer, R., Engeland, B., Stansfeld, C. and Pongs, O. (2000) Cloning and functional expression of rat eag2, a new member of the ether-a-go-go family of potassium channels and comparison of its distribution with that of eag1. *Mol. Cell. Neurosci.*, **16**, 59–70.
9. Schonherr, R., Gessner, G., Lober, K. and Heinemann, S.H. (2002) Functional distinction of human EAG1 and EAG2 potassium channels. *FEBS Lett.*, **514**, 204–208.
10. Ziechner, U., Schonherr, R., Born, A.K., Gavrilova-Ruch, O., Glaser, R.W., Malesevic, M., Kullertz, G. and Heinemann, S.H. (2006) Inhibition of human ether a go-go potassium channels by Ca2+/calmodulin binding to the cytosolic N- and C-termini. *FEBS J.*, **273**, 1074–1086.
11. Goncalves, J.T. and Stuhmer, W. (2008) Calmodulin interaction with hEAG1 visualized by FRET microscopy. *PLoS One*, **5**, e10873.
12. Ludwig, J., Terlau, H., Wunder, F., Bruggemann, A., Pardo, L.A., Marquardt, A., Stuhmer, W. and Pongs, O. (1994) Functional expression of a rat homologue of the voltage gated either a go-go potassium channel reveals differences in selectivity and activation kinetics between the Drosophila channel and its mammalian counterpart. *EMBO J.*, **13**, 4451–4458.
13. Occhiodoro, T., Bernheim, L., Liu, J.H., Bijlenga, P., Sinnreich, M., Bader, C.R. and Fischer-Lougheed, J. (1998) Cloning of a human ether-a-go-go potassium channel expressed in myoblasts at the onset of fusion. *FEBS Lett.*, **434**, 177–182.
14. Ju, M. and Wray, D. (2002) Molecular identification and characterisation of the human eag2 potassium channel. *FEBS Lett.*, **524**, 204–210.
15. Pardo, L.A., del Camino, D., Sanchez, A., Alves, F., Bruggemann, A., Beckh, S. and Stuhmer, W. (1999) Oncogenic potential of EAG K(+) channels. *EMBO J.*, **18**, 5540–5547.
16. Hemmerlein, B., Weseloh, R.M., Mello de Queiroz, F., Knotgen, H., Sanchez, A., Rubio, M.E., Martin, S., Schliephacke, T., Jenke, M., Heinz Joachim, R. *et al.* (2006) Overexpression of Eag1 potassium channels in clinical tumours. *Mol. Cancer*, **5**, 41.
17. Agarwal, J.R., Griesinger, F., Stuhmer, W. and Pardo, L.A. (2010) The potassium channel Ether a go-go is a novel prognostic factor with functional relevance in acute myeloid leukemia. *Mol. Cancer*, **9**, 18.
18. Asher, V., Khan, R., Warren, A., Shaw, R., Schalkwyk, G.V., Bali, A. and Sowter, H.M. (2010) The Eag potassium channel as a new prognostic marker in ovarian cancer. *Diagn. Pathol.*, **5**, 78.
19. Mello de Queiroz, F., Suarez-Kurtz, G., Stuhmer, W. and Pardo, L.A. (2006) Ether a go-go potassium channel expression in soft tissue sarcoma patients. *Mol. Cancer*, **5**, 42.
20. Ding, X.W., Luo, H.S., Jin, X., Yan, J.J. and Ai, Y.W. (2007) Aberrant expression of Eag1 potassium channels in gastric cancer patients and cell lines. *Med. Oncol.*, **24**, 345–350.
21. Ding, X.W., Wang, X.G., Luo, H.S., Tan, S.Y., Gao, S., Luo, B. and Jiang, H. (2008) Expression and prognostic roles of Eag1 in resected esophageal squamous cell carcinomas. *Dig. Dis. Sci.*, **53**, 2039–2044.

22. Wadhwa, S., Wadhwa, P., Dinda, A.K. and Gupta, N.P. (2009) Differential expression of potassium ion channels in human renal cell carcinoma. *Int. Urol. Nephrol.*, **41**, 251–257.

23. Rodriguez-Rasgado, J.A., Acuna-Macias, I. and Camacho, J. (2012) Eag1 channels as potential cancer biomarkers. *Sensors (Basel, Switzerland)*, **12**, 5986–5995.

24. Pardo, L.A. and Suhmer, W. (2008) Eag1 as a cancer target. *Expert Opin. Ther. Targets*, **12**, 837–843.

25. Saganich, M.J., Machado, E. and Rudy, B. (2001) Differential expression of genes encoding subthreshold-operating voltage-gated K+ channels in brain. *J. Neurosci.*, **21**, 4609–4624.

26. Martin, S., Lino de Oliveira, C., Mello de Queiroz, F., Pardo, L.A., Stuhmer, W. and Del Bel, E. (2008) Eag1 potassium channel immunohistochemistry in the CNS of adult rat and selected regions of human brain. *Neuroscience*, **155**, 833–844.

27. Gomez-Varela, D., Kohl, T., Schmidt, M., Rubio, M.E., Kawabe, H., Nehring, R.B., Schafer, S., Stuhmer, W. and Pardo, L.A. (2010) Characterization of Eag1 channel lateral mobility in rat hippocampal cultures by single-particle-tracking with quantum dots. *PLoS One*, **5**, e8858.

28. Saganich, M.J., Vega-Saenz de Miera, E., Nadal, M.S., Baker, H., Coetzee, W.A. and Rudy, B. (1999) Cloning of components of a novel subthreshold-activating K(+) channel with a unique pattern of expression in the cerebral cortex. *J. Neurosci.*, **19**, 10789–10802.

29. Gurling, H.M., Kalsi, G., Brynjolfson, J., Sigmundsson, T., Sherrington, R., Mankoo, B.S., Read, T., Murphy, P., Blaveri, E., McQuillin, A. *et al.* (2001) Genomewide genetic linkage analysis confirms the presence of susceptibility loci for schizophrenia, on chromosomes 1q32.2, 5q33.2, and 8p21-22 and provides support for linkage to schizophrenia, on chromosomes 11q23.3-24 and 20q12.1-11.23. *Am. J. Hum. Genet.*, **68**, 661–673.

30. Dreixler, J.C., Bian, J., Cao, Y., Roberts, M.T., Roizen, J.D. and Houamed, K.M. (2000) Block of rat brain recombinant SK channels by tricyclic antidepressants and related compounds. *Eur. J. Pharmacol.*, **401**, 1–7.

31. Terstappen, G.C., Pula, G., Carignani, C., Chen, M.X. and Roncarati, R. (2001) Pharmacological characterisation of the human small conductance calcium-activated potassium channel hSK3 reveals sensitivity to tricyclic antidepressants and antipsychotic phenothiazines. *Neuropharmacology*, **40**, 772–783.

32. Gavrilova-Ruch, O., Schonherr, K., Gessner, G., Schonherr, R., Klapperstuck, T., Wohlrab, W. and Heinemann, S.H. (2002) Effects of imipramine on ion channels and proliferation of IGR1 melanoma cells. *J. Membr. Biol.*, **188**, 137–149.

33. Garcia-Ferreiro, R.E., Kerschensteiner, D., Major, F., Monje, F., Stuhmer, W. and Pardo, L.A. (2004) Mechanism of block of hEag1 K+ channels by imipramine and astemizole. *J. Gen. Physiol.*, **124**, 301–317.

34. Hille, B. (2001) *Ion Channels of Excitable Membranes*. Sunderland, MA, Sinauer Associates.

35. Llinas, R. and Sugimori, M. (1980) Electrophysiological properties of in vitro Purkinje cell somata in mammalian cerebellar slices. *J. Physiol.*, **305**, 171–195.

36. Ganetzky, B. and Wu, C.F. (1983) Neurogenetic analysis of potassium currents in Drosophila: synergistic effects on neuromuscular transmission in double mutants. *J. Neurogenet.*, **1**, 17–28.

37. Stengel, R., Rivera-Milla, E., Sahoo, N., Ebert, C., Bollig, F., Heinemann, S.H., Schonherr, R. and Englert, C. (2012) Kcnh1 voltage-gated potassium channels are essential for early zebrafish development. *J. Biol. Chem.*, **287**, 35565–35575.

38. Frank, P.G. and Lisanti, M.P. (2006) Zebrafish as a novel model system to study the function of caveolae and caveolin-1 in organismal biology. *Am. J. Pathol.*, **169**, 1910–1912.

39. Kalivas, P.W., Sorg, B.A. and Hooks, M.S. (1993) The pharmacology and neural circuitry of sensitization to psychostimulants. *Behav. Pharmacol.*, **4**, 315–334.

40. Nestler, E.J. (2001) Molecular neurobiology of addiction. *Am. J. Addict.*, **10**, 201–217.

41. Barr, A.M., Markou, A. and Phillips, A.G. (2002) A 'crash' course on psychostimulant withdrawal as a model of depression. *Trends Pharmacol. Sci.*, **23**, 475–482.

42. Swerdlow, N.R. and Geyer, M.A. (1993) Clozapine and haloperidol in an animal model of sensorimotor gating deficits in schizophrenia. *Pharmacol. Biochem. Behav.*, **44**, 741–744.

43. Russig, H., Murphy, C.A. and Feldon, J. (2005) Behavioural consequences of withdrawal from three different administration schedules of amphetamine. *Behav. Brain Res.*, **165**, 26–35.

44. Klemm, W.R. (1989) Drug effects on active immobility responses: what they tell us about neurotransmitter systems and motor functions. *Prog. Neurobiol.*, **32**, 403–422.

45. Joy, C.B., Adams, C.E. and Lawrie, S.M. (2006) Haloperidol versus placebo for schizophrenia. *Cochrane Database Syst. Rev.*, **9**, CD003082.

46. Gao, K., Kemp, D.E., Ganocy, S.J., Gajwani, P., Xia, G. and Calabrese, J.R. (2008) Antipsychotic-induced extrapyramidal side effects in bipolar disorder and schizophrenia: a systematic review. *J. Clin. Psychopharmacol.*, **28**, 203–209.

47. Qian, Y., Hitzemann, B. and Hitzemann, R. (1992) D1 and D2 dopamine receptor distribution in the neuroleptic nonresponsive and neuroleptic responsive lines of mice, a quantitative receptor autoradiographic study. *J. Pharmacol. Exp. Ther.*, **261**, 341–348.

48. Kanes, S.J., Hitzemann, B.A. and Hitzemann, R.J. (1993) On the relationship between D2 receptor density and neuroleptic-induced catalepsy among eight inbred strains of mice. *J. Pharmacol. Exp. Ther.*, **267**, 538–547.

49. Ferreira, N.R., Mitkovski, M., Stuhmer, W., Pardo, L.A. and Del Bel, E.A. (2012) Ether-a-go-go 1 (Eag1) potassium channel expression in dopaminergic neurons of basal ganglia is modulated by 6-hydroxydopamine lesion. *Neurotox. Res.*, **21**, 317–333.

50. Downie, B.R., Sanchez, A., Knotgen, H., Contreras-Jurado, C., Gymnopoulos, M., Weber, C., Stuhmer, W. and Pardo, L.A. (2008) Eag1 expression interferes with hypoxia homeostasis and induces angiogenesis in tumors. *J. Biol. Chem.*, **283**, 36234–36240.

51. Gomez-Varela, D., Zwick-Wallasch, E., Knotgen, H., Sanchez, A., Hettmann, T., Ossipov, D., Weseloh, R., Contreras-Jurado, C., Rothe, M., Stuhmer, W. *et al.* (2007) Monoclonal antibody blockade of the human Eag1 potassium channel function exerts antitumor activity. *Cancer Res.*, **67**, 7343–7349.

52. Pardo, L.A. and Stuhmer, W. (2008) Eag1: an emerging oncological target. *Cancer Res.*, **68**, 1611–1613.

53. Bock, P. (1979) Improved Nissl method to stain formaldehyde or glutaraldehyde-fixed material. *Acta Neuropathol.*, **46**, 243–244.

54. Rogers, D.C., Peters, J., Martin, J.E., Ball, S., Nicholson, S.J., Witherden, A.S., Hafezparast, M., Latcham, J., Robinson, T.L., Quilter, C.A. *et al.* (2001) SHIRPA, a protocol for behavioral assessment: validation for longitudinal study of neurological dysfunction in mice. *Neurosci. Lett.*, **306**, 89–92.

55. Jones, BJ, R.D. (1968) A rotarod suitable for quantitative measurements of motor incoordination in naive mice. *Naunyn Schmiedebergs Arch. Exp. Pathol. Pharmakol.*, **259**, 211.

56. Nadler, J.J., Moy, S., Dold, G., Trang, D., Simmons, N., Perez, A., Young, N.B., Barbaro, R.P., Piven, J., Magnuson, T.R. and Crawley, J.N. (2004) Automated apparatus for quantitation of social approach behaviors in mice. *Genes Brain Behav.*, **3**, 303–314.

57. Lister, R.G. (1987) The use of a plus-maze to measure anxiety in the mouse. *Psychopharmacology (Berl)*, **92**, 180–185.

58. Blumstein, L.K. and Crawley, J.N. (1983) Further characterization of a simple, automated exploratory model for the anxiolytic effects of benzodiazepines. *Pharmacol. Biochem. Behav.*, **18**, 37–40.

59. Burns, L.H., Annett, L., Kelley, A.E., Everitt, B.J. and Robbins, T.W. (1996) Effects of lesions to amygdala, ventral subiculum, medial prefrontal cortex, and nucleus accumbens on the reaction to novelty: implication for limbic-striatal interactions. *Behav. Neurosci.*, **110**, 60–73.

60. Reisel, D., Bannerman, D.M., Schmitt, W.B., Deacon, R.M., Flint, J., Borchardt, T., Seeburg, P.H. and Rawlins, J.N. (2002) Spatial memory dissociations in mice lacking GluR1. *Nat. Neurosci.*, **5**, 868–873.

61. Stiedl, O., Misane, I., Spiess, J. and Ogren, S.O. (2000) Involvement of the 5-HT1A receptors in classical fear conditioning in C57BL/6J mice. *J. Neurosci.*, **20**, 8515–8527.

62. Geyer, M.A., McIlwain, K.L. and Paylor, R. (2002) Mouse genetic models for prepulse inhibition: an early review. *Mol. Psychiatry*, **7**, 1039–1053.